Tribology Letters, Vol. 18, No. 2, February 2005 (© 2005)
DOI: 10.1007/s11249-004-1778-3

Fundamental studies of Au contacts in MEMS RF switches

S.T. Patton[a,*] and J.S. Zabinski[b]

[a]*University of Dayton Research Institute, Dayton, OH 45469-0168, USA*
[b]*Materials & Manufacturing Directorate, Air Force Research Laboratory, Wright-Patterson Air Force Base, OH 45433–7750, USA*

Received 14 June 2004; accepted 19 September 2004

Microelectromechanical systems (MEMS) radio frequency (RF) switches hold great promise in a myriad of commercial, aerospace, and military applications. However, there is little understanding of the factors determining the performance and reliability of these devices. Fundamental studies of hot-switched gold (Au) contacts were conducted using a micro/nanoadhesion apparatus as a switch simulator. Experiments were conducted in a well defined air environment under precisely controlled operating conditions. Fundamental properties were connected to performance with an emphasis on the effects of contact force and electric current on contact resistance (R), microadhesion, and reliability/durability. Electric current had the most profound effect on switch performance. Observations at low current (1–10 μA) include: (1) slightly higher R; (2) asperity creep; (3) high adhesion after rapid switching; (4) switch bouncing; and (5) reasonable durability. Conversely, observations at high current (1–10 mA) include: (1) slightly lower R; (2) melting; (3) no measurable adhesion; (4) less propensity for switch bouncing; (5) necking of contacts; and (6) poor reliability and durability due to switch shorting. Low current behavior was dominated by the propensity to form smooth surface contacts by hammering, which led to high van der Waals force. High current behavior was dominated by the formation of Au nanowires that bridge the contact during separation. Data suggest the presence of an adventitious film containing carbon and oxygen. Aging of the contacts in air was found to reduce adhesion.

KEY WORDS: MEMS, RF switches, micro/nanoscale adhesion, failure mechanisms, reliability, contact resistance

1. Introduction

1.1. Motivation

Microelectromechanical systems (MEMS) offer great promise for integration of sensors, actuators, signal processing, and communications. Miniature smart systems that interact with the physical world, perform computations, and communicate with other systems are the ultimate goals of MEMS technology [1,2]. However, the small size of MEMS devices results in large surface area to volume ratios, which increases the importance of surface forces to the point where they dominate performance [3,4]. MEMS switches/relays are an example of a promising new technology that requires control over surface forces. Reliable making and breaking of electrical contact requires contact forces that typically range from a few μNs to as high as about a mN.

Little data exists on the microscale contact behavior of prospective electrode materials at MEMS-level forces [5]. Further understanding of microscale contact physics, chemistry, and mechanics is needed to develop the required reliability. The primary objective of this paper is to provide a fundamental understanding of microscale Au contacts. Such knowledge is also applicable to other technology areas such as simple pressure contacts used in connectors, sockets, and chip holders, which are becoming an increasing source of problems as the numbers of inputs/outputs increase and apparent contact sizes decrease [6].

*To whom correspondence should be addressed.
E-mail: steve.patton@wpafb.af.mil

1.2. Advantages of MEMS switches over current technologies

MEMS switches offer significant performance enhancement over current electromechanical (EM) and solid state (SS) switch technologies [7–16]. They show promise in a number of commercial, aerospace, and military applications with radio frequency (RF) applications being particularly promising [2]. Advantages of MEMS switches include: (1) high linearity; (2) low insertion loss; (3) low power consumption; (4) reduced size; (5) high shock resistance; (6) wider temperature range; (7) good isolation; and (8) low cost [1,7,9–26]. However, high switching voltage, relatively slow switching speeds (compared to SS), low power handling, concerns about packaging, and questionable reliability/durability are areas of concern [7,11,15,16, 21–23]. The potential benefits of this technology have led to significant efforts on MEMS switches in industry, government, and academia, but many issues remain before they can be commercialized [5,15]. In

fact, MEMS microrelays must be as reliable as conventional relays to be commercially viable [5].

Among the switch technologies presently used in RF systems, EM relays offer the best high frequency performance in terms of low insertion loss, high isolation, and good power handling (up to several Watts), but are large, slow, expensive, and lack durability. Solid state switches [e.g., gallium arsenide (GaAs) field effect transistor (FET) and p-i-n diodes] offer chip level integration, small size, fast switching times, excellent durability, and low cost, but generally do not perform well in broadband applications, have high insertion loss, and poor isolation [2]. In choosing between EM and SS switching technologies, there is generally a trade off between the high frequency performance of EM and the size, low cost and switching speed of SS [2]. High losses in SS switches tend to nullify the size benefits due to the need for signal amplifiers, which increase power consumption and complexity [2]. The attraction of MEMS is that they offer the performance of EM switches with the size and low cost of SS switches [2,8,17].

1.3. Applications

Applications for MEMS switches include wireless/satellite communications, radar, automated test equipment, instrumentation, DC motor control, and automotive [2,8,13,21,22,26,27–29]. Applications in RF communications systems include phase shifters, digitized capacitor banks, system front-ends, phased array antennas, and handsets [7,9,12,30]. RF switches are particularly applicable to reconfigurable systems [7].

1.4. Fabrication

MEMS switches have been fabricated using various technologies such as bulk micromachining, surface micromachining, and LIGA [25]. Materials used include silicon, GaAs, quartz, silicon dioxide, silicon nitride, and various metals [31,32]. Both lateral and vertical contacts have been fabricated [26]. For vertical contacts, the cantilever and air bridge are the most common [7,33]. It has been reported that switches with lateral contacts are generally inferior to those with vertical contacts due to high sidewall roughness [2,26]. However, no systematic study has identified the ideal roughness parameters for optimal performance.

1.5. Actuation schemes

Actuation schemes include electrostatic, magnetic, and thermal [13,28,34]. Each scheme has its own set of problems: (1) high power requirements and slow switching speed for thermal; (2) high incompatible voltages for electrostatic; and (3) high complexity, cost, and power requirements for magnetic [12,13,20]. Electrostatic actuation is most commonly used, and actuation voltage is minimized through the use of a compliant bridge or cantilever. However, this also reduces the available restoring force and makes adhesion a bigger concern. Low actuation voltage is a stringent requirement in integrated circuit (IC) test and automotive applications [8]. Advantages of thermal and magnetic actuation are that they can provide mN-level forces and operate at IC compatible voltages [8,26,27].

1.6. Types of MEMS switches

There are two types of MEMS RF switches of interest: direct current (DC) and capacitive. DC switches have metal-to-metal contacts (typically Au-on-Au), are suitable for use from 0-6 GHz, and are used for low current (300 mA) applications [2,7,9,14,22,32]. Failure mechanisms include adhesion, welding, melting, and sudden unexplained increase in contact resistance (R). Capacitive switches with metal-to-dielectric contacts (typically Au-on-silicon nitride) are used at frequencies of 10 GHz and above [2,7,9,10,19,22,32]. Failure mechanisms include adhesion, self-actuation (above 2W RF power), and dielectric charging [7,15,19,22]. Contact lifetime is generally less of an issue with capacitive switches [2]. The focus of this article will be on the reliability, durability, and failure mechanisms of DC switches with Au contacts.

1.7. Electrode materials

Au is a logical choice as the contact material because it: (1) is easily deformed (under low load); (2) has a low propensity to form alien surface films; (3) has high melting point; (4) is efficient in propagating RF signal; (5) is monolithic microwave integrated circuit (MMIC) compatible; (6) is corrosion resistant; (7) has low resistivity; and (8) is easily deposited [2,13,20,26,35–38]. Au is the most commonly used contact material in low current macroswitches [35]. Au is typically deposited by sputtering, evaporation, or electroplating [39]. Other contact materials used (or being considered for use) in microswitches include doped polysilicon, nickel (Ni), aluminum (Al), rhodium (Rh), palladium (Pd), and platinum (Pt) [22,39–43].

The main problem with Au is its propensity for high adhesion, which may lead to failure if restoring forces are not large enough to break a contact [20]. For example, Au contacts suffer from high adhesion (0.3–2.7 mN) as compared to AuNi5 (0–0.3 mN) and Rh (0.1 mN) [5,37]. However, the reduction in adhesion for AuNi5 and Rh came at the cost of higher R. A fundamental understanding of the relationships

between contact force, adhesion, and R is needed for MEMS switch design [5]. For instance, the adhesion force between electrodes essentially determines the minimum restoring force and compliance of a microbridge or cantilever, which can affect contact force and minimum actuation voltage. This study attempts to provide information on these relationships for Au contacts.

Despite its nobility, nominally clean Au is known to have a thin layer of adventitious carbon on its surface that is residue from the cleaning process and/or is adsorbed due to exposure to air. For instance, it has been reported that there are 20–40 Å of adsorbed hydrocarbons on freshly cleaned Au [44,45]. These alien films reduce and/or prevent metallic contact and increase R, but may actually be beneficial by reducing adhesion [46]. Contact resistance of a few ohms is typical of surfaces contaminated with carbon [47–49]. Another source of carbon is thermal decomposition of organic vapors during switch operation [47–49]. Surface contaminants increase R over that of the constriction resistance, and are particularly problematic at low mechanical and electrical loads [50]. Other typical contaminants in electrical contacts include particles, corrosion products, friction polymers, organic solvents, lubricants, and silica [50]. Contaminants are generally nonconducting and reports have shown that tunneling is the dominant charge transfer mechanism for Au contacts in both air and dry nitrogen environments [45,46,51,52].

1.8. Arcing

Arcing or electrical breakdown are concerns in switch applications [36,37]. Arcing typically produces vaporization and wear of electrodes along with material transfer, and is typically classified as "opening" and "closing" [36]. Closing arc considerations are governed by a similitude law concerning the electrical breakdown of a gas filled gap with a uniform electric field [36,53]. It is expressed in Paschen's law as a relationship between the breakdown voltage (V_s) and the product of the pressure (p) and the gap width (s) in air at 20 °C. It is generally thought that closing arc is not critical for MEMS switches, but cannot be totally discounted due to deviations from Paschen's law at small separation [36,53,54].

Opening (Townsend or metal vapor) arc is initiated by either field emission of electrons or explosive evaporation at points of contact [36,54]. Opening arc, although of minor importance in macroswitches, may be important in MEMS switches and result in the transfer of material from the anode to cathode [54]. Bridge transfer is another wear mechanism that usually manifests itself as cavitation in the anode and elevation on the cathode [36]. Bridge transfer is closely related to opening arc, but material transfer is a result of hot spots (breaking points) in metal bridges being displaced from their center. There is limited understanding of the effects of arcing and bridge transfer on MEMS switches, and we hope to shed some light on these issues in this paper.

1.9. Contact resistance

Contact resistance should be as low as possible to reduce both Joule heating and signal (insertion) loss. Thermal management is critical for MEMS switch performance, and thermal modeling is an important component of the design process [40,45,55]. In RF applications, thermal effects and electron crowding due to the skin effect (concentration of current near the surface of a conductor) are a concern for power handling, particularly above 2 GHz [16]. Contact resistance is the sum of a constriction term and a film term. The constriction resistance, R_c, is a consequence of the current flow being constricted through small conducting spots, and for a single circular contact spot can be written as

$$R_c = \rho/2a, \tag{1}$$

where ρ is the resistivity of the contact material (for like contacts) and a is the radius of a circular contact area [36,56]. The film resistance (R_f) of a circular contact covered with a uniform film (e.g., alien film) can be written as

$$R_f = \frac{\rho_f d}{\pi a^2}, \tag{2}$$

where ρ_f is the film resistivity and d is the film thickness [36,56]. Although Equations. (1) and (2) are simplified, they do illustrate some key concepts. One is that more real area of contact (RAC) (larger a) reduces both R_c and R_f, and that the film thickness and resistivity are important for R_f. It should also be pointed out that quantum mechanical tunneling is a mechanism for charge transfer, and can reduce the film resistance when film thickness is on the order of a few angstroms [36].

MEMS switch designers need to know the relationship between R and contact force to effectively size components and forces to provide stable contact resistance at minimum force [44,57]. Contact resistance has been measured in past studies using actual MEMS switches, atomic force microscopes (AFMs), and an interfacial force microscope (IFM), among others [5,6,8,18,20,27,28,31,37,39,44,47,50,52,57–60]. One of the major problems with previous reports of R is a significant inconsistency in results. This may be due to different: (1) contact geometries; (2) sample cleaning

and storing methods; (3) operating environments; (4) contact forces/pressures; and (5) electrical loads (i.e., current and voltage). In most instances, the precise conditions of the studies are not reported, which makes data interpretation and comparison difficult.

A number of previous studies have reported R at various contact force. Unless otherwise specified, we will limit our discussion to Au–Au contacts. The results vary from study-to-study, and were conducted using different apparatus in either air (at various RH), dry nitrogen, or unspecified environments [20,27,28,31, 37,39,44,45,50,52,57–62]. Reported minimum R varied from less than 100 mΩ to several ohms at loads from 25 μN to 300 mN.

The complexity of R behavior at various contact force is illustrated in the following. Using an AFM with Au–Au contacts in air, several contact cycles were needed to initiate current flow (to scrape away an insulating film), and then conduction increased, but subsequent behavior included loss of conduction and intermittent high resistance [6,58]. Generally, contact resistance was independent of load [6,58]. A study on MEMS switches with Au contacts at loads up to 300 μN found: (1) R of about 20 Ω; (2) slight dependence of R on load; and (3) a significant dependence of R on current with R decreasing with increasing current [62]. However, the test environment was not reported, which significantly limits the value of the data. IFM studies on Au contacts in dry nitrogen at loads of 30 μN and below found a range of R from 10 Ω to 10^5 Ω with many failed attempts to establish electrical contact [45]. The preceding two reports illustrate that contact resistance behavior of Au contacts at MEMS-scale loads is not well understood.

1.10. Failure mechanisms and durability

Early failure is one of the primary concerns associated with MEMS switches, but published reports of their reliability/durability are scarce [63]. Further complicating the problem is that many of the studies were conducted in different environments at different currents, loads, and switching modes (i.e., hot or cold) without efforts to correlate data to test environment. In hot switching, the signal flows through the contact until the contact breaks mechanically as opposed to cold switching where the signal is turned on and off only when the electrodes are engaged [39]. The most commonly mentioned failure mechanisms are adhesion, welding, and a mysterious sudden increase in R during cycling, but rigorous study of the underlying causes of failure is missing [17,34,52,59,63]. A number of studies have reported problems (e.g., shorting and welding) related to the softening and/or melting of Au electrodes [26,27,31,34,37,50,63]. This is intimately related to the power-handling capability of MEMS switches, which is limited by current density considerations [10,32]. The maximum allowable current for Au contacts has been reported to be from 20 to 500 mA in nitrogen, air, and unreported environments [27,28,31,34,37,52,59].

Durability is important and is often expressed as the number of cycles to failure [1,20,22,27, 28,30,31,34,35,63]. However, the number of cycles to failure is not meaningful unless operation conditions (e.g., current, voltage, force, switching mode, and environment) are specified. For instance, MEMS switch lifetimes have been reported to be anywhere from 10^3 to 10^9 cycles, but switching mode, operating parameters and environment were not completely specified [17,20,22,30]. The switching mode affects durability, with hot switched contacts having been reported to have less durability than cold switched contacts [27,63]. Current was reported to have an adverse effect on durability with lifetime decreasing up to three orders of magnitude at currents above 10 mA [1,34]. Hot-switched lifetime at 10 mA improved by six orders of magnitude in nitrogen, but reasons for improved lifetime in N_2 compared to air was not given [1]. Another study suggested that durability in N_2 would be better than in air [31], but did not elaborate as to why this was expected. Another observation is reduced and more stable R with cycling, but has only been observed in a couple of studies [8,20]. Clearly, failure mechanisms, reliability, durability, and current handling of Au contacts at MEMS-scale loads are not well understood with widely varying behavior reported in previous studies.

The objectives of this investigation were to conduct fundamental studies of hot-switched Au contacts using a micro/nanoadhesion apparatus as a switch simulator. An emphasis was placed on relationships between contact force, electric current, R, microscale adhesion, and reliability/durability in a well defined environment and precisely controlled operating conditions. Results of this study are relevant to contact electrodes in MEMS switches, and provide design input to MEMS switch designers.

2. Experimental

2.1. Micro/nanoadhesion apparatus and test procedure

A micro/nanoadhesion apparatus [4] was modified to allow R measurement in this study. A detailed discussion of microscale force measurement and experimental procedures for adhesion measurement was published earlier [4]. However, we will briefly review key aspects of the apparatus and experimental methods as well as discuss modifications that were made for this study. The instrument uses a ball-on-flat configuration. Au was coated onto balls and wafers, which were then used in experiments. Design features include:

(1) fine control of ball position; (2) control of electric current flow; (3) measurement of MEMS scale forces (~1 μN and above); and (4) measurement of R. The apparatus allows us to quickly screen switch contact materials for adhesion, R, separation mode (e.g., brittle or ductile), and performance/reliability/durability. It also eliminates time consuming and expensive device-level fabrication and testing for all but the most promising electrode materials.

A block diagram schematic of the experimental apparatus is given in figure 1. The environmental chamber allows control of temperature and relative humidity (RH), and experiments were conducted in air at 22 ± 1 °C and 45 ± 5%RH. A constant current source was used to drive DC current through the ball-to-wafer contact, and a simple voltage divider was used as the contact resistance circuit. The range of currents used in experiments was 10 μA to 10 mA. A series resistor of 1 kΩ and a four-wire configuration were used to measure contact voltage. It was shown previously that both signal loss and power-handling performance of MEMS switches with DC current is representative of the same performance at RF frequencies [30,39]. Other aspects of switch performance may differ between DC and RF, especially in regards to electromigration, which is not an issue at RF frequencies [64]. Results given here are fully applicable to DC operation of MEMS switches. It is also reasonable to expect that DC results at low current, where electromigration is not a concern, should be representative of the RF case at low current.

Two types of experiments were conducted, adhesion and rapid switching. In adhesion experiments, a triangle wave input signal was applied to the actuator, which resulted in a constant approach and retract speed of 320 nm/s for the ball. In rapid switching experiments, a 5 Hz square wave signal with a displacement amplitude of 1.6 μm was used. The maximum force on the wafer varied from 20 μN to 1 mN, which corresponds to wafer displacements from 10 nm to 500 nm. The range of maximum mean Hertzian contact stresses (radii) was from about 15 MPa (0.7 μm) to about 50 MPa (2.5 μm). Pure plastic analysis yields a range of contact radii from about 0.1 μm to about 0.8 μm. During switching experiments, actuator input signal (ball position), conditioned adhesion signal, and contact voltage were sampled using an analog to digital converter and stored in a personal computer.

2.2. Test specimens and characterization

Polished GaAs wafers were coated with Au and diced into 100 mm^2 area squares for switching experiments. A combination of sputtering and electroplating was used to coat wafers. A 200 Å thick titanium (Ti) bond layer was first sputtered onto the wafer. This was followed by a film stack of: (1) 700 Å of sputtered Au; (2) 4 μm of electroplated Au; and (3) 700 Å of sputtered Au. The Au stack was used on the wafer to give the model contact the same structure as films used in actual MEMS switches, where plated Au is a structural material and sputtered Au is the electrode material. Au was also sputtered onto 1.6 mm diameter Grade 100 440C stainless steel balls. A 200 Å thick Ti bond layer was first sputtered onto the ball followed by 1 μm of sputtered Au. Wafer and ball specimens were cleaned before testing by subjecting them to ultrasonic cleaning separately in hexane, acetone, and methanol for 5 min each, and were then dried at 55 °C on a hot plate. Optical microscopy, scanning electron microscopy (SEM), and AFM were used to inspect and characterize virgin and worn electrode surfaces.

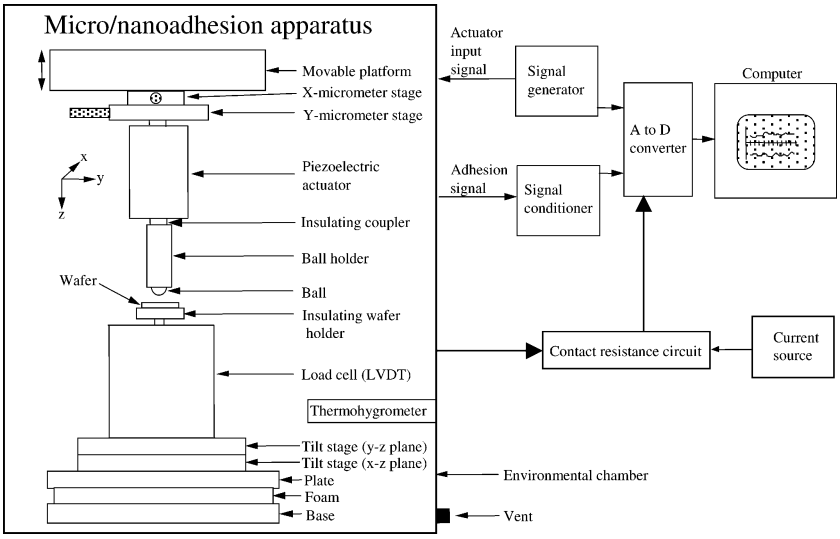

Figure 1. Schematic of the micro/nanoadhesion apparatus and associated instrumentation used in RF MEMS switch simulation studies.

The rms roughness of the Au-coated wafers and balls were 17.6 and 13.6 nm, respectively, as measured by AFM at a 10 μm $\times$ 10 μm scan area.

It is important to comment on the relevance of our ball-on-flat contact geometry to true MEMS switch contacts. In actuality, the typical contact geometry in MEMS switches is planar [8,13,17,26,27,31,34,37, 59,62,63], which may be by design or due to the fact that contact dimples that are designed to be spherical on top end up being flat or "donut shaped" on top leading to unanticipated contact geometry. Even if spherical dimples are made, they will flatten while in contact or due to permanent deformation from repeated contacts. Apparent contact area (A_a) varies from 1 to 500 μm^2 in various studies of planar MEMS DC switch contacts [8,13,17,26,27,31,34,37,59,62,63], while A_a varies from about 3 to 1000 μm^2 in this study. Apparent area of contact in our simulated contact is thus comparable to that in actual MEMS switches. Au films used here are identical to those used in MEMS switches, so roughness effects should be the same in the actual and simulated cases. Since our A_a and roughness are similar to true MEMS, our adhesion results for Au contacts are applicable MEMS switches with Au contacts. Wear effects are applicable to MEMS switches for the same reasons.

3. Results and discussion

3.1. Adhesion experiments

Our first goal was to understand contact behavior in a simple adhesion experiment. Figure 2 shows force and contact resistance versus time curves for a Au-coated ball against a Au-coated wafer during a microadhesion experiment. The force is recorded as positive being down ($+z$ direction), see coordinates in figure 1. The wafer displacement scale shown in figure 2 was obtained from calibration data [4], and is a measure of wafer motion during an experiment. In this particular experiment, the maximum force was about 200 μN. This kind of experiment is typically used for adhesion measurement [4], and consists of: (1) an approach segment (0–0.2 s); (2) a contact segment (0.2–1.05 s); and a retract segment (1.05–1.25 s). No adhesion was observed in figure 2, which is typical for hot switching experiments at and above 1 mA. If adhesion was present, force would become negative during the retract segment just before separation.

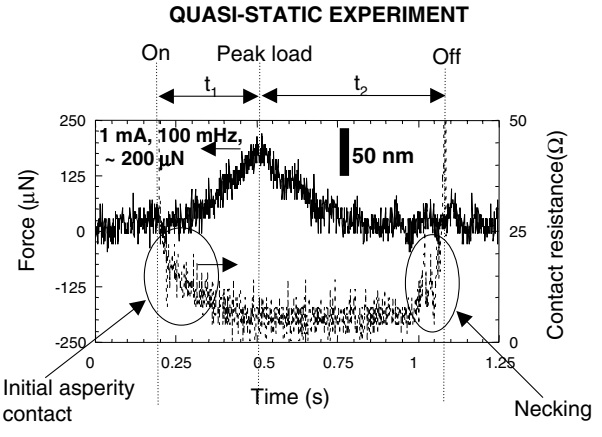

Figure 2. Force and contact resistance versus time curves for an Au-coated ball against a Au-coated wafer at 1 mA (high) current. This kind of experiment at a constant approach and retract speed of 320 nm/s was used to determine adhesion. The key points to emphasize are: (1) no adhesion was measured under these conditions; (2) there was a quick decrease in contact resistance due to high current density and asperity melting; (3) necking delayed contact breakage; and (4) there was no load dependence for contact resistance over t_2.

Aspects of high current (1–10 mA) switching can be ascertained from figure 2. It should be noted that currents greater than 10 mA led to contact instability and burn out. Power dissipation is about 1 mW at 10 mA, which appears to be the power-handling limit of our configuration. The first observation in figure 2 is that necking (plastic deformation) occurred since t_2 (time interval from peak force to loss of electrical contact) is greater than t_1 (time interval from initial electric contact to peak force). If necking had not occurred, electrical contact should have ceased around 0.75–0.8 s. The second observation is that there is a rapid decrease in R during the initial asperity contacts (from 0.2 to 0.45 s). At first, current flows through a relatively small number of contacts. This leads to high current density and asperity melting. Since the molten metal cannot resist the applied load, there is relative displacement between the contacts [36]. This process ends when sufficient load bearing area is established to pass the current in a solidified state. Another interesting fact is that R is relatively constant from about 0.5 to 1 s, even though the load changes considerably during this time interval. Thus, R is independent of load (over the load range shown) until the contact is broken. This kind of behavior is possible if asperity welding keeps contact area constant as the compressive force is removed [36]. Similar behavior was observed during indentation experiments that used a tungsten tip against a nickel flat in UHV [65,66]. Plastic deformation can also lead to greater contact area during unloading than during loading [67], and the fact that R remains low and constant as the compressive force is removed in figure 2 indicates that this may be the case here.

Low current (1–10 μA) behavior is illustrated in figure 3, which shows the effect of current on contact force and voltage. From here onward in this paper, we will designate low current as being from 1 to 10 μA, and high current as being from 1 to 10 mA. Points A, B, and C correspond to the establishment of electrical contact, peak force ($\sim$200 μN), and the breaking of electrical contact, respectively. Clearly, the interaction between electrodes is different at high and low current.

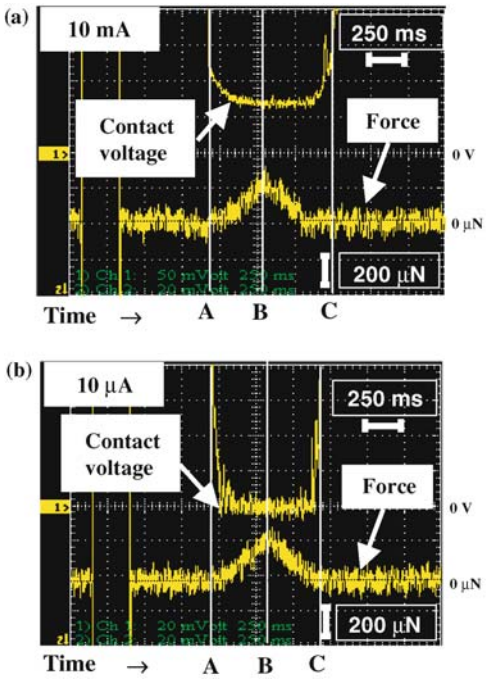

Figure 3. Oscilloscope traces showing contact voltage and contact force versus time during adhesion experiments conducted at (a) 10 mA, and (b) 10 μA. Ductile separation occurred at high current (10 mA), whereas, brittle separation occurred at low current (10 μA).

Necking or ductile type separation occurred at 10 mA, and brittle type separation occurred at 10 μA. Electrical contact was broken when force returned to 0 μN at 10 μA, but not at 10 mA. Time segments AB and BC differ by only about 7% at 10 μA (AB = 350 ms, BC = 325 ms), but BC is 24% larger than AB at 10 mA (AB = 375 ms, BC = 475 ms). Generally, brittle behavior was observed at low current, and ductile behavior was observed at high current. Detailed analysis of separation modes at metal microcontacts is given in an earlier study [68]. Data in figure 3(b) is consistent with a brittle type separation mode at maximum contact radius [68], whereas, high current in figure 3 (a) leads to a ductile type separation mode that is not well characterized in the literature.

3.2. Contact resistance

Monitoring R as a function of time provides information on the temporal behavior of the contact because R is related to real area of contact (RAC). Figure 4(a) shows contact resistance as a function of time. In these experiments, the ball was loaded against the wafer at 200 μN, and then R was measured as a function of time with the ball position being held fixed. The first observation is that the steady state value of R is on the order of a few ohms over the range of current tested. This suggests that the contact was not metallic and was being dominated by quantum mechanical tunneling through an alien thin film from a

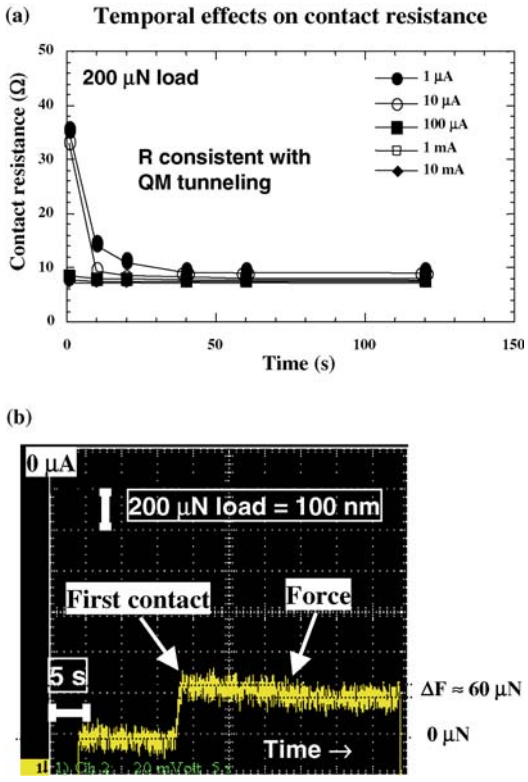

Figure 4. (a) Contact resistance versus time at a load of 200 μN. Temporal effects were observed only at low current with contact resistance decreasing to a steady state value in about a minute. Asperity creep was responsible for temporal effects at low current, but creep was prevented by asperity melting at high current. (b) Oscilloscope trace showing force versus time during an experiment where a 200 μN load was applied at 0 μA. The force relaxes, which implies wafer motion towards the fixed ball, and is accompanied by increased real contact area and lower contact resistance.

few angstroms to perhaps a few tens of angstroms thick [36]. A time dependence to R was observed only at low current, and R decreased rapidly in the first few seconds and reached a steady state after about 40 s. The decrease in R indicates an increase in the RAC. The increase in RAC can only occur via asperity creep. Creep was observed at μN-level normal forces in one other study that used Au balls [69]. Although the effect of current was not investigated in that earlier study [69], it can be ascertained from their work that the current was less than or equal to 100 μA. Silver–nickel electrical contacts were also studied previously [70], and they found asperity creep, force relaxation, and decreased contact resistance over a few hours time at 50 mA current and 50 g force. Our data is unique in showing that creep does not occur at all levels of current for Au contacts.

Creep was not observed at high current. High current density in the tallest asperities led to melting and quick establishment of large contact area capable of carrying the current in a solidified state, see figure 2. The larger contact area prevented creep due to less stress at asperity contacts. Although the concept of

asperity melting to form large contact area is known, its prevention of creep has not, to our knowledge, been previously reported. We also note that there is a slight dependence of R on current (in the steady state) with higher current giving slightly less R. The mild current dependence is consistent with the low voltage (10 μV to 100 mV here) tunneling behavior of 5–30 Å thick films between metallic contacts [36]. By mild current dependence we mean changes in R of less than about 25%, as opposed to possible changes by orders of magnitude in going from very low voltage ($\sim$0 V) to about 2 V [36]. Another viewpoint is that the small increase in R with current is indicative of a negative temperature coefficient of resistivity, which indicates that the contact is behaving as a semiconductor [47]. Although not explicitly pointed out, a previous study showed a decrease in R with increasing current [46].

To further support our hypothesis of creep at low current, we carefully monitored the temporal behavior of contact force. Figure 4(b) shows the relaxation of contact force for a contact loaded to about 200 μN at 0 μA current. Similar behavior was observed at low current. After first contact, the ball position was held constant. Relaxation of the contact force indicates wafer movement towards the fixed ball position. This is consistent with asperity creep and increased contact area. The total force relaxation [ΔF in figure 4(b)] was about 60 μN, which corresponds to about 25 nm of wafer motion. Figure 5 shows a simplified schematic of the contact experiment. For illustrative simplicity, we have depicted the ball as ideally smooth in contact with a rough wafer surface. As in the actual experiment, the wafer is attached to a spring (load cell), which itself is attached to a fixed base. Schematic cross-sectional views of the contact showing qualitative real areas of contact are also given. The following argument applies to the cases of zero or small current.

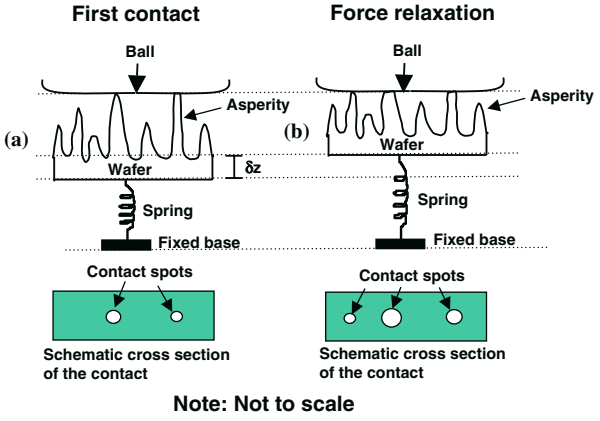

Figure 5. Schematic illustration of the mechanism of force relaxation in a zero or low current contact. Although the initial asperity deformation is enough to support the load, time dependent creep effects lead to additional asperity deformation, which allows the spring force to relax.

At first contact, asperities deform enough to support the load. After the initial asperity deformation, contacting asperities are under compressive strain and are susceptible to creep. Creep is accompanied by spring relaxation and displacement (δz) as well as increased contact area as shown in figure 5. Increased contact area leads to decreased R. It should be noted that increased contact area is consistent with higher contact stiffness [67], which decreases deformation response to loading. The model in figure 5 along with data in figure 4 offer solid reasoning and data to support the hypothesis that creep decreases R at low current.

Aside from temporal effects, the effects of current and contact load on R is of fundamental importance. Figure 6(a) shows the effects of load and current on R. These are steady state values taken after R had stabilized in each condition. Contact resistance decreases as current increases, but the effect saturates at 100 μA. At each current, the effect of load on R is minimal. At least two other studies have observed minimal load dependence of R using Au contacts [6,62]. At high current, lack of load dependence can be explained by the fact that the contact area (and hence R) is dominated

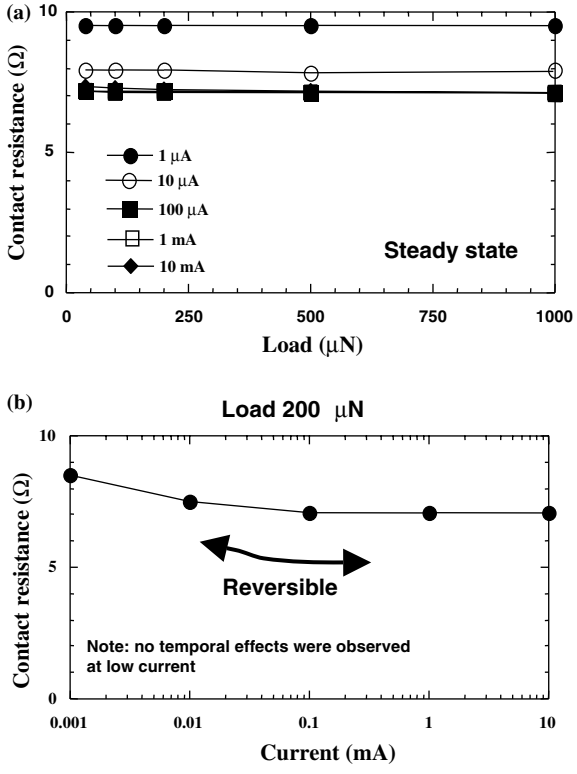

Figure 6. (a) Steady state contact resistance versus load at various current. Contact resistance decreased with current, but the effect saturates at 100 μA. The effect of load on contact resistance is minimal. (b) Effect of current on contact resistance. Contact was first made at 10 mA, and then current was changed without breaking the contact. Lack of temporal effects at low current indicates constant contact area during the experiment. The decreasing nature of contact resistance versus current indicates that a thin tunnel conducting film dominated contact behavior.

by melting, and the role of the load during melting is to simply move the surfaces closer together. The decrease in R with increased current is not unexpected if quantum mechanical tunneling through an alien film is the charge transfer mechanism [36]. More current increases voltage across the contact by Ohms Law. Voltage shifts the Fermi level up by the product eV (where e is the electron charge and V is the voltage) on one side of the film barrier, which allows a net tunneling current to flow [36].

To further investigate the nature (metallic or tunnel conducting) of contacts, we performed a classic experiment suggested by Holm [36]. Figure 6(b) shows the results. Contact was first made at 200 μN and 10 mA, and then the current was changed without breaking the contact. The initial high current of 10 mA led to high current density, melting, plastic deformation, and increased real contact area. The idea is to establish a large contact area first, and then to vary the current at fixed contact area. If R goes up as current increases, then the contact is metallic [36]. If R goes down as current increases, then the contact is tunnel conducting [36]. Contact resistance followed the curve in figure 6(b) and was reversible as current was changed, which is an indication that contact area was indeed constant during the experiment. Also supporting constant contact area is the fact that there were no temporal effects at low current under these conditions. This was not the case in figure 4(a) where time effects were observed at 1 and 10 μA. The decreasing nature of R versus current in figure 6(b) indicates that contact behavior is dominated by a thin tunnel conducting film [36]. This does not exclude the possibility that some fraction of the contact is metallic, but simply indicates that overall it is acting as a tunnel conductor.

3.3. Surface analysis

Auger electron spectroscopy (AES) was used to analyze the surface of freshly cleaned Au-coated wafers, and data are presented in figure 7. The spectrum shows Au peaks along with C and O peaks from surface contamination. These species may be residue from the cleaning process or adsorbed from air. Hydrocarbons and carbon dioxide are examples of air-borne species that may have adsorbed onto the surface [4]. Data in figure 7 are presented as chemical evidence of an alien film on the surface of Au electrodes.

3.4. Adhesion creation

Up to now, we have shown only the lack of adhesion at high current. However, during our study we discovered large adhesion under some experimental conditions. We will now describe some interesting observations. Much to the surprise of the authors,

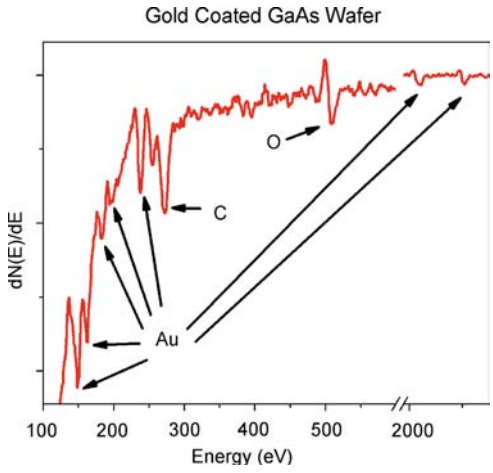

Figure 7. Auger electron spectra of a freshly cleaned Au wafer. Data suggest coverage of the wafer surface with species containing carbon and oxygen.

rapid switching of the contacts at zero or low current (0–10μA) was the only way to produce measurable adhesion. Figure 8(a) shows an example of this phenomenon. At first, this was puzzling as one may expect more adhesion at high current from welding. Contacts, which at first showed no signs of adhesion, were cycled using a 5 Hz square wave at 100 μN and 1 μA for 5 min. Immediately after cycling, adhesion experiments were conducted, and the results are shown in figure 8a, where adhesion is about 150 μN. Apparently, the hammering during rapid cycling changed the surfaces in a way that promotes adhesion. If the current was subsequently increased to 100 μA or more during an adhesion experiment, then adhesion was annihilated as

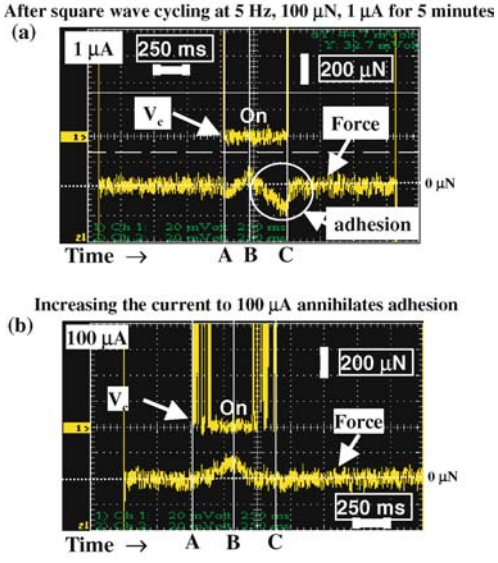

Figure 8. (a) Oscilloscope trace showing contact voltage and contact force versus time during an adhesion experiment conducted after square wave cycling at 5 Hz, 100 μN, and 1 μA for 5 min. Cycling at low current creates adhesion. (b) Oscilloscope trace taken immediately after the experiment in (a), but with the current turned up to 100 μA. High current annihilates adhesion.

shown in figure 8(b). Thus, high current can neither create adhesion during rapid switching nor allow adhesion to exist. The reason for this is that current affects surface morphology of the contacts. To our knowledge, low current hammering as an adhesion creation mechanism, and lack of adhesion at high current, are new observations and concepts for the literature.

An optical microscope was used to inspect surfaces created during low current cycling. Figure 9 shows the surface of a ball that was run for 60 min at 5 Hz, 1 μA, and 100 μN. The circled area in figure 9 shows a smoothened ball surface, as there is less diffuse reflection where the ball was contacting the wafer. This is essentially a case of asperity blunting by hammering. The smoothened surface reduced spacing between the ball and wafer and led to high van der Waals force.

This phenomenon can be better understood by considering some well known equations. The attractive van der Waals force for a ball versus flat contact can be written as

$$F = \frac{AR}{6D^2}, \tag{3}$$

where A is the Hamaker constant ($\sim 3 \times 10^{-19}$ J for Au), R is the ball radius, and D is the distance between the ball and flat [71]. This is for a smooth ball and flat, and any surface roughness (minus deformation) will increase separation. If a facet or localized flat area forms on the ball, the van der Waals force for a smooth flat versus flat contact may be more relevant. The attractive van der Waals force per unit area for a planar contact can be written as

$$\frac{F}{\text{area}} = \frac{A}{6\pi D^3}. \tag{4}$$

Some simple analyses can be performed using these equations. The induced adhesion in figure 8(a) is about 150 μN. Using this and $R = 0.8$ mm in Equation (3), we get $D = 5.2$ Å. This suggests intimate contact and smoother surface contacts, which is shown in figure 9.

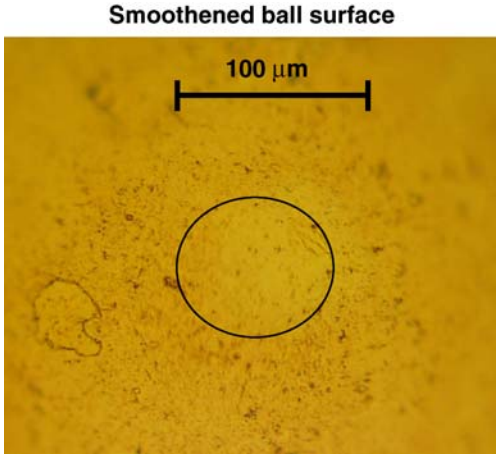

Figure 9. Optical micrograph of a virgin ball surface after cycling at 5 Hz, 1 μA, and 100 μN for 60 min. Hammering at low current creates a smooth ball surface.

3.5. Aging

A critical parameter that is often overlooked in adhesion experiments is the effect of aging, particularly for samples exposed to air. Figure 10 shows that aging in air reduces adhesion. The series of adhesion experiments was conducted at zero current. Figure 10(a) shows about 300 μN of adhesion that was created by cycling for 1 h at 5 Hz, 100 μN, and 0 μA. No adhesion was present before this cycling. Aging the contacts in air for twelve hours (overnight) reduced the adhesion to about 200 μN, as shown in figure 10(b). Based on our previous work [4] and common knowledge in surface science, adventitious hydrocarbons and other species adsorb onto a surface over time. Using Equation (3), we find that the separation increased from 3.7 to

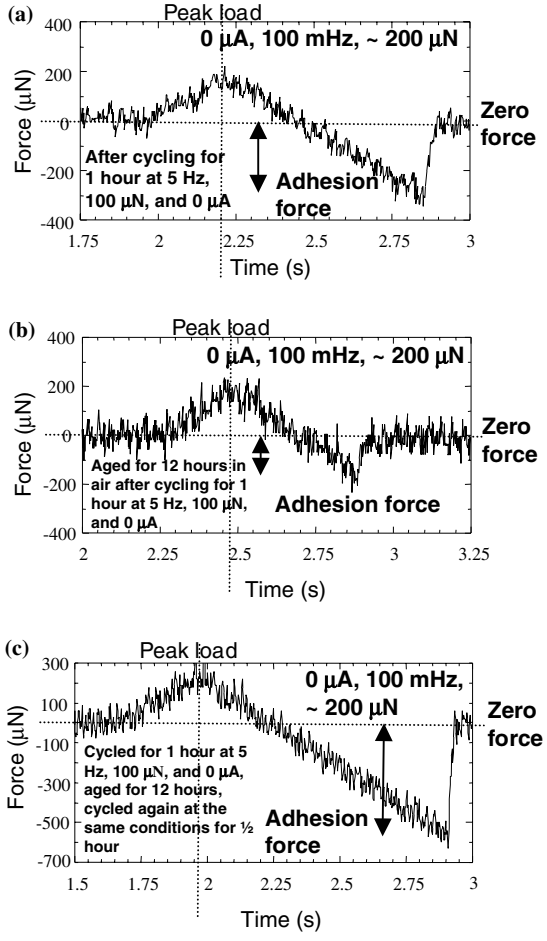

Figure 10. Force versus time during adhesion experiments conducted at 0 μA, 100 mHz, and ~200 μN force during the following sequence of events: (a) after cycling for 1 h at 5 Hz, 100 μN, and 0 μA; (b) then aged for 12 h in air; and (c) then cycled for 30 min at 5 Hz, 100 μN, and 0 μA. Aging in air reduces adhesion.

4.5 Å as force decreased from 300 to 200 μN. This suggests that a film of average thickness of an angstrom or more adsorbed onto the surface overnight. This adsorbed film thickness is consistent with adventitious carbon growth on single crystal silicon wafers [4]. Finally, continued cycling of the contact after aging leads to an even higher adhesion of about 550 μN in figure 10(c). Figure 10 reinforces the concept that cycling at low (or zero) current produces adhesion, and also shows that aging in air and the likely passivation of the contacts with adventitious species reduces adhesion. A likely mechanism is increased surface separation and reduced van der Waals interaction.

3.6. Dynamic experiments

In this section, we will discuss the performance of switch contacts during rapid switching experiments conducted at 5 Hz, ~100 μN, and various current. Experiments conducted at high current are discussed first. One of our first objectives was to determine the minimum force needed for efficient switch operation. Figure 11(a) shows an example where the force was too low, as not all attempts to turn the switch on were successful. In this case, the force is not measurable by our sensor. The situation is remedied in figure 11(b), where a force of about 100 μN was used and switching operation was excellent. We found that 100 μN was sufficient force to operate the switch, and no advantage in performance was gained at higher forces. However, providing sufficient force does not guarantee problem free operation. For example, there is an inherent instability in the force at 1 mA and above. The instability, shown in figure 11(c) in the circled area, is an intermittent increase in the contact force. The instability is an indication that the wafer was pushed down farther than normal, since the measured force is simply kz where k is the spring constant of the force sensor and z is the downward displacement of the wafer from its equilibrium position.

Since the force instability is simply an indication of farther downward displacement of the wafer, we considered mechanisms that allowed for this behavior. Figure 12 shows such a mechanism that can explain the force instability. The nominal force level is determined by the position of the ball at maximum penetration with respect to the equilibrium position of the wafer. In figure 12(a), z_1 is the displacement of the wafer from equilibrium at maximum ball penetration, and kz_1 is the nominal force level. If material flows by electromigration (migration of the metal atoms due to momentum transfer from conduction electrons) from the cathode to the anode, then the separation could be increased to z_2 due to the interposing material as shown in figure 12(b). To transmit the additional force, the interposing material between electrodes must

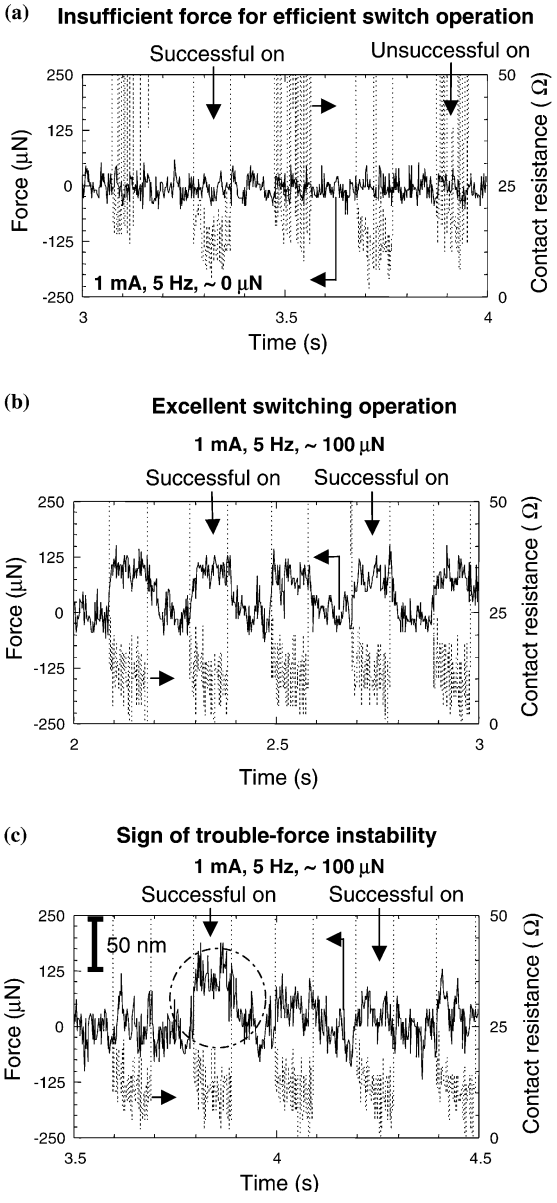

Figure 11. Force and contact resistance versus time during rapid switching experiments at 1 mA and very low force. (a) Force was insufficient for efficient switch operation as not all attempts to turn the switch on were successful. (b) Excellent switching operation was attained at 100 μN. (c) Although the switch is operating reliably, a sign of trouble in the form of a force instability is seen. Note the wafer displacement scale.

become solid during loading. Evidence of electromigration is shown in the SEM image of a ball surface run to failure at 10 mA in figure 12(c). Localized melting (note change in grain structure) and interposing material are readily seen.

An unfortunate effect of the force instability is that it is a prelude to switch shorting, which is the primary failure mechanism at high current. This is shown in figure 13(a). The instability begins at about 1.95 s, where the force increased from about 150 μN to over 300 μN. From about 1.95 to 3.1 s, the switch remained

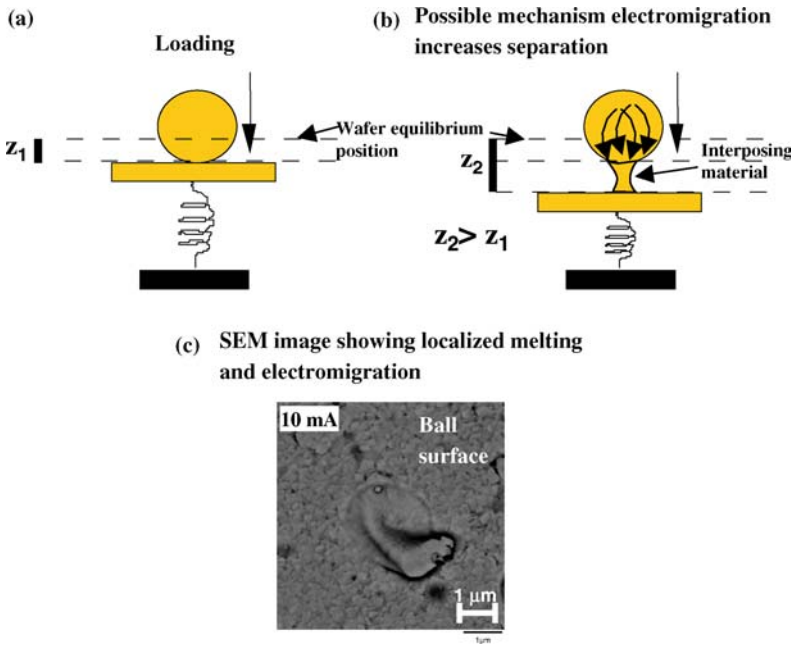

Figure 12. (a) and (b) Schematics illustrating how electromigration causes the observed force instability at high current (above 1 mA). (c) SEM image showing localized melting and electromigration on a ball run to failure at 10 mA.

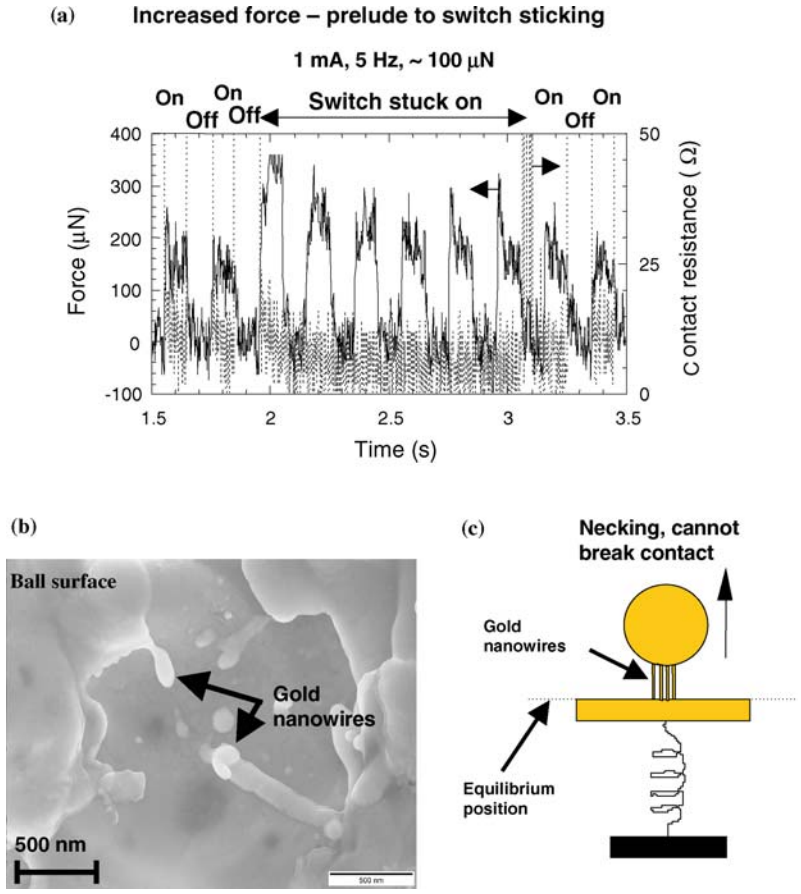

Figure 13. (a) Force and contact resistance versus time during rapid switching experiments at 1 mA and about 100 μN force. Increased force is a prelude to the switch sticking on and failure. (b) SEM image showing nanowire formation on a failed ball surface run to failure at 1 mA. (c) Schematic illustration showing how nanowires can bridge the contact during ball retraction thereby shorting the switch.

on despite the fact that five attempts were made to turn it off. The inability to reliably switch upon demand is our failure criteria, which is satisfied by the behavior in figure 13(a). Once this kind of behavior shows up in an experiment, it continues to appear intermittently thereby malfunctioning. This is essentially failure by short circuiting of the switch. During routine inspection of the contacts, we discovered that nanowires were responsible for switch failure. Figures 13(b) and (c) show Au nanowires on a Au ball run to failure at 1 mA along with a schematic illustration of the failure mechanism. In the SEM image in figure 13(b), in addition to the Au nanowires there is evidence of melting and metal spatter that occurred in an explosive process as the nanowires were drawn out. Figure 13(c) summarizes the proposed mechanism. Even though the ball is retracted to the point that there is no geometric interference with the wafer in its equilibrium position, Au nanowires bridge the contact maintaining physical and electrical contact. Although AFM has been used to study conduction and plastic deformation in Au nanowires [72], their presence in MEMS switch contacts has not been reported previously. Melting or even vaporization of Au nanowires occurs as wire diameter decreases as the wire is drawn out. This leads to higher current density and Joule heating, and confirms that one of the preludes to opening arc occurs at 1 mA and above. We observed elevation on the cathode at 1 mA and above, which could have been caused by opening arc and/or bridge transfer. Adhesion annihilation at high current [see figure 8(b)] is due to nanowire formation and associated surface roughening.

Failure by nanowire formation did not occur at low current. A minimum current density in asperity contacts is apparently needed to form nanowires. The shapes of the force and contact resistance curves during rapid switching at low current differ from those at high current. Figure 14 shows force and contact resistance curves during rapid switching experiments at 10 μA. The main feature in the graph is the spike in the force curve upon loading, an example of which is labeled as "bounce" in figure 14. This bounce past the nominal maximum penetration of the ball is due to the initial collision. This result suggests that if bounce is a concern for MEMS switches, it is most likely to occur at low current. Contact bounce was observed in actual MEMS switches at high actuation voltage, although the current was not given [17]. One very important observation in the literature is that conditions favorable for weld formation (e.g., high current) decreased bouncing in macroswitches [36]. The weld presumably provides adherence that prevents the movable electrode from separating from the fixed electrode. This is consistent with our findings as well.

Further inspection of used ball surfaces offers insight into failure mechanisms. Figure 15 shows optical,

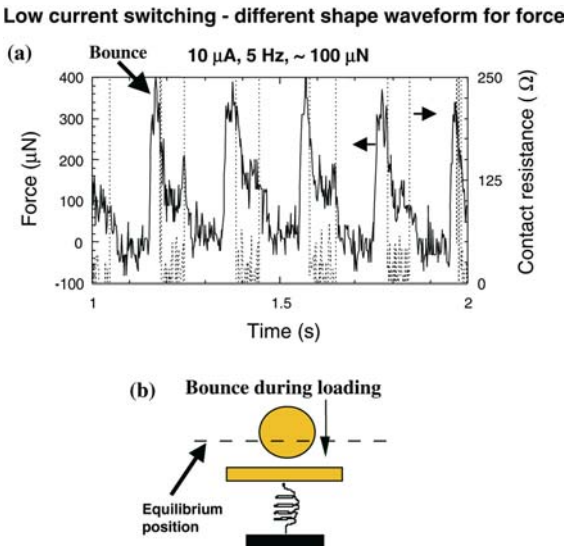

Figure 14. (a) Force and contact resistance versus time during rapid switching experiments at 10 μA and about 100 μN force. Low current switching led to a different shape waveform for force due to switch bouncing. (b) Schematic illustration of switch bounce during loading.

SEM, and 3-D profilometer images of Au ball surfaces run to failure at 5 Hz, 100 μN, and high current. A prominent wear mark is seen in all cases. Melting is seen in the interior of the wear mark, and is visible in figure 15(a) along with a perimeter region where nanowires are present [see figure 13(b) for high magnification view of nanowires]. If the switch is further cycled for an hour at 5 Hz, 100 μN, and 1 μA (low current), then a smooth surface is created on the perimeter of the wear mark as seen in figure 15(b). It is this smooth surface and increased van der Waals force that are likely responsible for high adhesion after cycling at low current, see figures 8 and 10. This progression of events only makes sense if the perimeter region of the wear mark is higher than the center region. This is shown in figures 15(c) and (d), where we focus on the raised perimeter in (c), and directly show the raised perimeter in (d). The flat smooth surface in figure 15(b) is about 10 μm^2 in area. Using this area and a separation of about 4 Å in Equation (4), we obtain a force of about 2.5 mN. As seen in figure 10(c), we observed adhesion forces approaching a mN in our experiments. These back of the envelope calculations seem to support the hypothesis that van der Waals force is the primary cause of adhesion in these experiments.

This brings us to the subject of reliability/durability. Figure 16 shows the number of cycles to failure as a function of current. All experiments were conducted at 5 Hz and about 100 μN. At and above 1 mA, failure occurred after about 1000 cycles due to intermittent shorting. At and below 0.1 mA, switches were run for over 10^5 cycles without failing by shorting. However, adhesion and switch bouncing are concerns at low

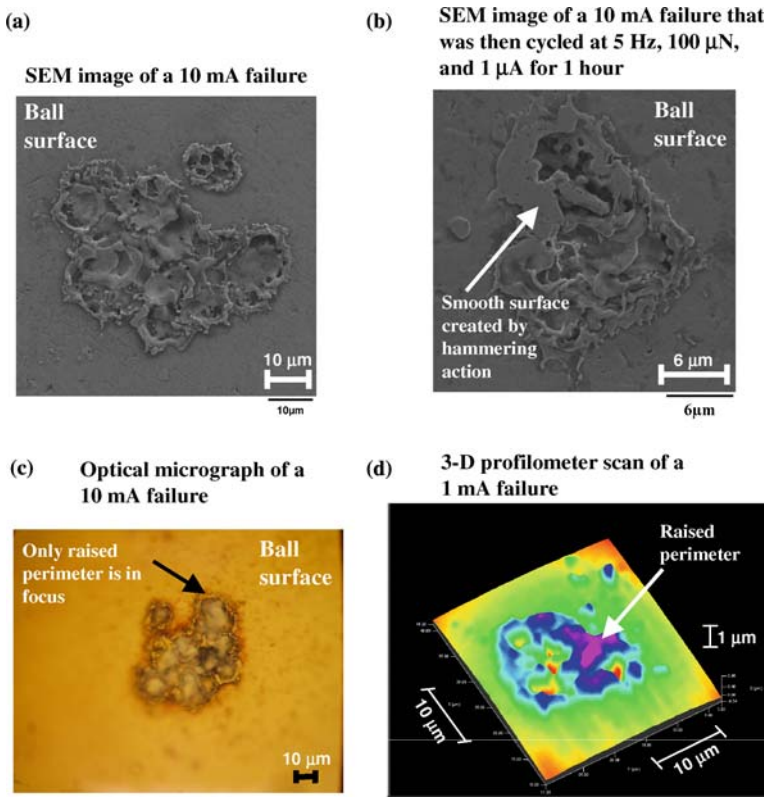

Figure 15. Optical, SEM, and 3-D profilometer images of ball surfaces run to failure at 5 Hz, 100 μN, and 1–10 mA. In (b), the switch was further run for an hour at 5 Hz, 100 μN, and 1 μA.

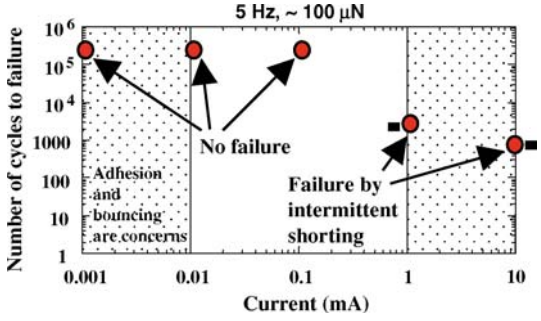

Figure 16. Switch reliability/durability at various currents in air at 45% RH. At high current (≥1 mA), switches failed after about 10^3 cycles by intermittent shorting. At low current, failure by shorting was not observed, but adhesion and bouncing are concerns.

current. Current plays an important role in determining reliability/durability, with contacts being less reliable/durable at higher current. Current is also known to be a primary influence on contact lifetime in macroswitches, with lifetime decreasing at higher current [35].

4. Summary

Fundamental experiments investigating MEMS RF Au switch contacts were conducted under precisely controlled operating conditions in air at MEMS-scale forces using a modified microadhesion apparatus. An emphasis was placed on the role of surface forces and electric current on switch performance, reliability, and durability. From a reliability and switch burnout perspective, current handling was effectively limited to about 10 mA. Electric current had a profound effect on deformation mechanisms, adhesion, R, and reliability/durability. Asperity creep, slightly higher R, switching induced adhesion, and switch bouncing were present at low current. Asperity melting, slightly lower R, near zero adhesion, poor durability, and switch shorting by nanowire formation were present at high current. Contact resistance values, decreasing R with current, and the presence of a film containing carbon and oxygen suggest that tunneling was the dominant charge transfer mechanism at both low and high current. Adhesion was linked to the creation of a smooth surface texture and associated van der Waals forces. Surface roughening by nanowire formation prevented adhesion at high current. A number of the observations and mechanisms brought forth in this paper are new, and are expected to provide input to MEMS designers to improve performance and reliability.

Acknowledgments

The authors thank Kevin Leedy of the Air Force Research Laboratory, Sensors Directorate for Au deposition. We also thank Steven Smallwood and Josekutty Nainaparampil of Universal Technology Corporation for Auger and AFM measurements, respectively.

References

[1] P.M. Zavracky, S. Majumder and N.E. McGruer, IEEE J. Micromech. Syst. 10 (1997) 511.
[2] J.J. Yao, J. Micromech. Microeng. 10 (2000) R9.
[3] M. Madou, *Fundamentals of Microfabrication* (CRC Press, Boca Raton, 1997).
[4] S.T. Patton, K.C. Eapen and J.S. Zabinski, Tribol. Int. 34 (2001) 481.
[5] J. Schimkat, Sens. Actuat. A 73 (1999) 138.
[6] J. Beale and R.F. Pease, IEEE Trans. Comp. Pack. Manufact. Technol. A 17 (1994) 257.
[7] E.R. Brown, IEEE Trans. Microwave Theory Tech. 46 (1998) 1868.
[8] W.P. Taylor, O. Brand and M.G. Allen, IEEE J. Micromech. Syst. 7 (1998) 181.
[9] N.S. Barker and G.M. Rebeiz, IEEE Trans. Microwave Theory Tech. 46 (1998) 1881.
[10] Z.J. Yao, S. Chen, S. Estelman, D. Denniston and C. Goldsmith, IEEE J. Micromech. Syst. 8 (1999) 129.
[11] S.P. Pacheco, L.P.J. Katehi and C.T.C. Nguyen, IEEE MTT-S Inter. Microwave Symp. Proc. (2000) 165.
[12] D. Hah, E. Yoon and S. Hong, IEEE Trans. Microwave Theory Tech. 48 (2000) 2540.
[13] X. Lafontan, F. Pressecq, G. Perez, C. Pufaza and J.M. Karam, Proc. SPIE. 4558 (2001) 11.
[14] J.Y. Park, G.H. Kim, K.W. Chung and J.U. Bu, Sens. Actuat. A 89 (2001) 88.
[15] J. Wellman, Technology readiness overview: RF MEMS switches, NASA Electronic Parts and Packaging Program, March, 2003.
[16] B.D. Jensen, K. Saitoh, J.L. Volakis and K. Kurabayashi, Presented at the 6th ASME-JSME Therm. Engineer. Joint Conf. Hawaii Island, Hawaii, 6–11 June, 2003.
[17] K.E. Peterson, IBM J. Res. Devel. 23 (1979) 376.
[18] S. Majumder, N.E. McGruer, P.M. Zavracky, G.G. Adams, R.H. Morrison and J. Krim, in: *Tribology Issues and Opportunities in MEMS*, ed., B. Bhushan (Kluwer Academic Publishers, Dordrecht, 1998) p. 471.
[19] C.L. Goldsmith, Z. Yao, S. Eshelman and D. Denniston, IEEE Microwave Guided Wave Lett. 8 (1998) 269.
[20] I. Schiele, J. Huber, B. Hillerich and F. Kozlowski, Sens. Actuat. A 66 (1998) 345.
[21] A. Malczewski, S. Eshelman, B. Pillans, J. Ehmke and C.L. Goldsmith, IEEE Microwave Guided Wave Lett. 9 (1999) 517.
[22] C.T.C. Nguyen, L.P.B. Katehi and G.M. Rebeiz, Proc. IEEE 86 (1999) 1756.
[23] V. Sieracki, Presented at the 2000 DARPA AOC Radar and EW Conference, Laurel, Md, 25–26 October, 2000.
[24] D. Balaraman, S.K. Bhattacharya, F. Ayazi and J. Papapolymerou, IEEE MTT-S Inter. Microwave Symp. Proc. (2002) 1225.
[25] H.F. Schlaak, Proc. 21st Conf. Electr. Cont. (2002) 19.
[26] Y. Wang, L. Zhiyong, D.T. McCormick and N.C. Tien, Sens. Actuat. A 103 (2003) 231.
[27] J.A. Wright, Y.C. Tai and G. Lilienthal, Proc. Solid State Sens. Actuat. Workshop (1998) 304.
[28] M. Ruan, J. Shen and C.B. Wheeler, IEEE J. Micromech. Syst. 71 (2001) 491.
[29] R. Allan, Electronic Design Online (2002) ID#2138, Available-from:URL:http://www.elecdesign.com/Articles/Index.cfm?ArticleID = 2138.
[30] D. Hyman, A. Schmitz, B. Warneke, T.Y. Hsu, J. Lam, J. Brown, J. Schaffner, A. Walston, R.Y. Loo, G.L. Tangonan, M. Mehregany and J. Lee, Electron. Lett. 35 (1999) 224.
[31] Z. Li, D. Zhang, T. Li, W. Wang and G. Wu, J. Micromech. Microeng. 10 (2000) 329.
[32] G. Rebeiz, Short Course, Presented at Wright-Patterson Air Force Base, OH, June, 2002.
[33] J.M. Kim, C.W. Baek, J.H. Park, D.S. Shin, Y.S. Lee and Y.K. Kim, J. Micromech. Microeng. 12 (2002) 688.
[34] J.A. Wright and Y.C. Tai, NARM Relay Conf. (1998) 13–1.
[35] Anonymous, Available from: URL:http://relays.tycoelectronics.com/schrack/pdf/relay_basics.pdf.
[36] R. Holm, *Electric Contacts* (Springer-Verlag, New York, 1967).
[37] E.J.J. Kruglick and K.S.J. Pister, IEEE J. Micromech. Syst. 8 (1999) 264.
[38] L.E. Larson, R.H. Hackett and R.F. Lohr, Proc. 6th Intl. Conf. Solid-State Sens. Actuat. (1999) 743.
[39] D.J. Hyman, Ph.D. dissertation, Case Western Reserve University, 2000.
[40] M.A. Gretillat, P. Thieboud, C. Linder and N.F. de Rooij, J. Micromech. Microeng. 5 (1995) 156.
[41] J. Yao and M. Chang, Proc. 8th Intl. Conf. Solid-State Sens. Actuat. (1995) 384.
[42] S. Hannoe and H. Hosaka, Microsyst. Technol. 3 (1996) 31.
[43] M.A. Gretillat, F. Gretillat and N.F. de Rooij, J. Micromech. Microeng. 9 (1999) 324.
[44] D. Hyman and M. Mehregany, IEEE Trans. Comp. Pack. Technol. 22 (1999) 357.
[45] J. Tringe, W. Wilson and J. Houston, Proc. SPIE 4558 (2001) 151.
[46] J.W. Tringe, T.A. Uhlman, A.C. Oliver and J.E. Houston, J. Appl. Phys. 93 (2003) 4661.
[47] C.N. Neufeld and C.N. Rieder, IEEE Trans. Comp. Pack. Manufact. Technol. A 18 (1995) 399.
[48] H.P. Koidl, W.F. Rieder and Q.R. Salzman, Proc. 43rd IEEE Holm Conf. Electr. Cont. (1997) 328.
[49] H.P. Koidl, W.F. Rieder and Q.R. Salzman, Proc. Forty-Forth IEEE Holm Conf. On Electr. Cont. (1998) 220.
[50] C.N. Neufeld and C.N. Rieder, IEEE Trans. Comp. Pack. Manufact. Technol. A 18 (1995) 369.
[51] A. Tonck, F. Houze, L. Boyer, J.L. Loubet and J.M. Georges, J. Phys.: Cond. Matt. 3 (1991) 5195.
[52] S. Majumder, N.E. McGruer, G.G. Adams, A. Zavracky, P.M. Zavracky, R.H. Morrison and J. Krim, Proc. 44th IEEE Holm Conf. Electr. Cont. (1998) 127.
[53] P.G. Slade and E.D. Taylor, IEEE Trans. Comp. Pack. Technol. 25 (2002) 390.
[54] E.J.J. Kruglick, Ph.D. dissertation, University of California, Berkeley, 1999.
[55] C.H. Leung, A. Lee and B.J. Wang, IEEE Trans. Comp. Pack. Manufact. Technol. A 19 (1996) 346.
[56] S. Schoft, J. Kindersberger and H. Lobl, Proc. 21st Conf. Electr. Cont. (2002) 230.
[57] D. Hyman and M. Mehregany, Proc. 44th IEEE Holm Conf. Electr. Cont. (1998) 133.
[58] J.P. Beale and R.F.W. Pease, Proc. 38th IEEE Holm Conf. Electr. Cont. (1992) 45.
[59] I. Schiele and B. Hillerich, J. Micromech. Microeng. 9 (1999) 146.
[60] M. Raun and J. Shen, Proc. 47th IEEE Holm Conf. Electr. Cont. (2001) 224.
[61] H. Hosaka, H. Kuwano and K. Yanagisawa, Proc. IEEE MEMS Conf. (1993) 12.
[62] X. Lafontan, C. Dufaza, M. Robert, G. Perez and F. Pressecq, Proc. SPIE 4175 (2000) 149.

[63] D. Becher, R. Chan, M. Hattendorf and M. Feng, Presented at the GaAs MANTECH Conf., San Diego, CA, 8–11 April, 2002.
[64] J. Tao, J.F. Chen, N.W. Cheung and C. Hu, IEEE Trans. Electron Devices 43 (1996) 800.
[65] M.D. Pashley, J.B. Pethica and D. Tabor, Wear 100 (1984) 7.
[66] M.D. Pashley and J.B. Pethica, J. Vac. Sci. Technol. A 3 (1985) 757.
[67] R.S. Dwyer-Joyce, B.W. Drinkwater and A.M. Quinn, ASME J. Tribol. 123 (2001) 8.
[68] D. Maugis and H.M. Pollock, Acta Metal. 32 (1984) 1323.
[69] R. Budakian and S.J. Putterman, Phys. Rev. B 65 (2002) 235429.
[70] C. Poulain, L. Boyer, P. Sainsot, M.H. Maitournam, F. Houze, M. Leclercq, J.P. Guery and J.P. Charpentier, Proc. 41st IEEE Holm Conf. Electr. Cont. (1995) 147.
[71] J.N. Israelachvili, *Intermolecular and Surface Forces* (Academic Press, San Diego, 1992).
[72] P.E. Marszalek, W.J. Greenleaf, H. Li, A.F. Oberhauser and J.M. Fernandez, PNAS 97 (2000) 6282.